Adsorption performances of nickel oxide nanoparticles (NiO NPs) towards bromophenol blue dye (BB)

Hatem A. Al-Aoh

Department of Chemistry, Faculty of Science, University of Tabuk, 71474 Tabuk, Saudi Arabia, Tel. +965 6 537692007;
email: issa_hatem2@yahoo.com

abstract

In this research, the microwave-assisted method was used for the synthesis of nickel oxide nanoparticles (NiO NPs). The synthesized NiO NPs were characterized using Brunauer–Emmett–Teller surface analyzer, transmission electron microscopy, X-ray diffraction and pH_{ZPC}. We found that the specific surface area, total pore volume, average pore diameter and pH_{ZPC} of the prepared NiO NPs were 78.37 m^2/g, 0.068 cm^3/g, 34.92 Å and 8.1. Also, we examined the adsorption of Bromophenol blue (BB) using NiO NPs at different temperatures (303, 318 and 333 K). Further, we evaluated the impacts of adsorbate concentration, agitation time, temperature and pH. Indeed, the adsorbate concentration of 300 mg/L, temperature of 333 K and pH of 12 at 24 h were observed to be the ideal experimental conditions. Isotherm models of Freundlich and Langmuir were employed and the obtained results revealed that the equilibrium data were described well by Langmuir equation. The highest monolayer capacities of this adsorption were found to be 58.48, 79.37 and 93.46 mg/g at 303, 318 and 333 K. Kinetic models of first order, second order and intra-particle diffusion were used to examine the kinetic experimental data. Thermodynamic factors were determined and the values obtained designate that the adsorption of BB on NiO NPs is endothermic and non-spontaneous processes.

Keywords: Adsorption; Isotherm; Kinetics; Thermodynamics; Nickel oxide nanoparticles; Bromophenol blue dye

1. Introduction

Bromophenol blue (BB) is an anionic organic dye [1,2] that has sufficient ability for making direct bands with basic functional groups in the components of tissues [3]. The BB dye is applied as a colour mark to check the colouring proteins in paper electrophoresis, the process of agarose gel electrophoresis and polyacrylamide gel electrophoresis [3]. Moreover, the dye of BB is used as pH indicator because the colour of this dye solution depends on the values of solution pH. For instance, the solution of BB is blue and yellow at neutral and lower pH, respectively [3]. A dye of BB as a bromophenol organic compound has teratogenic, toxic and carcinogenic properties [4]. Thus, the industrial effluents polluted by this dye have negatives and hazard impacts on the ecosystem. Therefore, effective method is highly needed for removal of dye from waste water. For instance, Yu-Juan and Xi-Hai [1] have studied the efficiency of solvent sublation method to eliminate the BB from wastewaters. The dye removal efficiency of solvent sublation technique is negligible at higher pH solution [2] and also has a potential secondary contamination, which would be produced due to using of solvents. Further, photocatalytic degradations using potassium dichromate ($K_2Cr_2O_7$) [3], cobalt-doped TiO_2 nanoparticles [4], $NiTiO_3$ and TiO_2 under UV–Vis light [5], CuO-nano-clinoptilolite [6] and TiO_2 nanoparticles [7] have been employed to minimize the BB dye from synthesized wastewaters. Despite, the considerable efficiency of the photocatalytic degradation method, its final products may be having significant negative impact on human health when compared with BB dye itself. Thus, it is very important to find out the best and the most effective method can be applied

for the quantitative elimination of BB dye from manufacturing wastewaters prior their discarding to biosphere. It was recommended earlier that adsorption is the best and most effective method has been used till now for removal of the coloured dyes from industrial wastewaters. For this, adsorption was chosen in this work for elimination of BB from the prepared wastewater.

Activated carbon prepared from *Astragalus bisulcatus* was reported for the adsorption of BB from synthesized wastewater [8]. However, it was reported that this activated carbon has a great potential towards BB removal, the production cost of activated carbon is quite expensive. Consequently, low-cost adsorbents such as graphene oxide functionalized magnetic [9] and α-chitin nanoparticles have been used for the adsorption of dyes from wastewaters.

Adsorption of organic dyes such as methylene blue (MB) on biomass-derived carbon@montmorillonite nanocomposites was performed by Ai and Li [10]. Further, Dhananasekaran et al. [11] highlighted that the chitosan composite effectively removed BB dye from wastewater. Indeed, removal of BB from wastewaters was reported using adsorbents such as polymeric gels [12], mesoporous mixture gel [13] and ionic liquids [14]. It was noted that the adsorption efficiency of the above mentioned low-cost adsorbents towards BB is negligible when compared with high-cost activated carbon. Recently many attempts have been carried out to use the composite materials such as CuS nanoparticles–loaded activated carbon [15], Fe_2O_3–ZnO–$ZnFe_2O_4$/carbon nanocomposite [16] and polymer–clay composite [17] as new effective adsorbents for purification of wastewaters from BB dye. It was concluded that the composite materials have effective application as BB dye removal from aqueous solutions. Unfortunately, the chemicals used for the preparation of this type of adsorbents are expensive and harmful to environment. Therefore, metal oxides nanoparticles have been employed as effective and cheap adsorbents for removal of organic and inorganic hazard materials from wastewaters. For example, CuO NPs were used for adsorption of mercury (II) [18] as same as adsorption of ethidium bromide and ethidium monoazide bromide from aqueous solution [19]. Further, maghemite nanoparticles of γ-Fe_2O_3 were used as adsorbent for elimination of fluoride ions from its aqueous solution [20]. Furthermore, MgO nanoparticles and ZnO–MgO nanocomposites are effective adsorbents for linezolid antibiotic [21]. Also, alumina NPs [22] and Sorel's cement [23] have been applied for elimination of BB from wastewater. In addition, Hu et al. [24] observed that NiO NPs had high adsorption capacity and adsorption rate towards Congo red (CR). Isotherm and kinetic parameters for adsorption of CR on NiO NPs were investigated by Zheng et al. [25] and found that NiO NPs has superior adsorption performance with CR. Lei et al. [26] noted that NiO–SiO_2 composite particles were used as great adsorbents for elimination of CR from wastewater, with adsorption capacity of 204.1 mg/g. Moreover, adsorption of anionic dyes such as methyl orange, methyl blue and CR was carried out by Shao and Huang [27]. They found that NiO NPs can be applied as an effective adsorbent for removal of dyes from aqueous solutions. Despite superior adsorptive properties of NiO NPs towards organic dyes, no work till now was performed to study BB adsorption onto NiO NPs. Consequently, the real goal of current research is to examine the elimination performance of this adsorbent (NiO NPs) towards BB.

Parameters of kinetics, thermodynamics and isotherms of BB adsorption onto NiO NPs were estimated. Experimental factors affecting adsorption such as temperature, BB solution concentration, shaking time and pH of the solution were also investigated.

2. Research methodologies

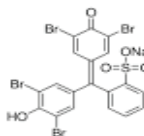### 2.1. Production and characterization of NiO NPs

A microwave oven with 650 W power (Sanle General Electric Corp., Nanjing, China) was used. In a typical procedure, 25 mL water solution containing 0.2 M $Ni(NO_3)_2 \cdot 6H_2O$ was mixed with a 25 mL water solution containing 0.2 M $CO(NH_2)_2$ in a round-bottom flask. The vessel containing the solution was introduced into a microwave oven operating at a maximum power of 800 W for 20 min. The solution boils and undergoes dehydration followed by decomposition with the evolution of a large amount of gases. After the solution reaches the point of spontaneous combustion, it begins burning and releases lots of heat, vaporizes all the solution instantly, and becomes a solid powder [28,29]. A black fine powder of NiO NPs is extracted. After cooling to room temperature, the precipitate was centrifuged and washed with distilled water. The final products were collected for characterization.

Powder X-ray diffraction (XRD) measurements were performed on a Shimadzu XD-3A X-ray diffractometer at the 2θ range from 30° to 60°, with monochromatized CuKα radiation (λ = 0.15418 nm). The transmission electron microscopy (TEM) images were recorded on a JEM 200CX (JEOL, USA) transmission electron microscope, using an accelerating voltage of 80 kV. The samples used for TEM observations were prepared by dispersing some products in ethanol followed by ultrasonic vibration for 30 min, then placing a drop of the dispersion onto a copper grid coated with a layer of amorphous carbon. Theydan and Ahmed [30] method was followed in this study to determine pH_{ZPC} of this adsorbent. The surface area and porosity of NiO NPs were evaluated by adsorption–desorption of N_2 at 758.58 mm Hg and 77.40 K using Brunauer–Emmett–Teller (BET) surface analyzer (NOVA-3200 Ver. 6.09).

2.2. Experimental solutions of BB

Table 1 includes characteristics of BB dye. This dye was supplied by Sigma-Aldrich, United States. 1 g of BB was dissolved in distilled water in a 1 L volumetric flask to prepare

Table 1
Structure and characteristics of BB dye

Structure	Other names	CI number	λ_{max} (nm)	M_w (g/mol)
	Aristolochic acid	45,170	598	624.38

1,000 mg/L of stock solution. The required experimental solutions were obtained from stock solution by dilution.

2.3. Adsorption experiments

To examine impacts of adsorbate primary concentration, temperature of solution, isotherm and thermodynamic parameters, BB adsorption on NiO NPs was performed at three different temperatures (30°C, 44°C and 60°C) with concentrations of the dye solutions in the range of 35–600 mg/L by means of 0.02 g of NiO NPs. These experiments were carried out at agitation speed 200 rpm and initial pH for 72 h to reach stability. The adsorbents were separated from solutions filtration. Remaining BB concentrations in the supernatant liquids were evaluated using 6800 UV-visible spectrophotometer (Jenway, UK) at λ_{max} of 598 nm. The quantities of BB adsorbed at equilibrium were computed from the following equation:

$$q_e = \frac{(C_i - C_e)V}{m} \tag{1}$$

C_i and C_e (mg/L) represent the primary and final BB concentrations, in that order, m (g) is related to the mass of NiO NPs, q_e is the number of grams of BB adsorbed by 1 g of the adsorbent at equilibrium, whereas V (L) represents the adsorbate solution volume.

The Langmuir and Freundlich linear forms models (Eqs. (2) and (3)) have been applied to determine parameters of the adsorption isotherms.

$$\frac{C_e}{q_e} = \frac{1}{q_{max} K_L} + \frac{C_e}{q_{max}} \tag{2}$$

$$\ln q_e = \ln K_F + \frac{1}{n} \ln C_e \tag{3}$$

q_{max} refers to the maximum adsorption capacity (mg/g); K_L represents constant of Langmuir; K_F and $1/n$ are Freundlich constants correlated to adsorption capacity and favourability, respectively. Adsorption is favourable when the value of $1/n$ lies between 0 and 1 [31].

The dimensionless factor R_L represented by Eq. (4) [32] was applied to investigate the fundamental characteristics of Langmuir isotherm model:

$$R_L = \frac{1}{1 + K_L C_i} \tag{4}$$

K_L and C_i are the Langmuir constant and highest primary concentration of adsorbate. R_L value designates the isotherm nature, either favourable (R_L between 1 and 0), unfavourable (R_L higher than 1), linear (R_L equal to 1) or irreversible (R_L equal to 0).

Eqs. (5) and (6) were used to investigate the thermodynamic factors such as $\Delta H°$, $\Delta S°$ and $\Delta G°$ for BB adsorption onto NiO NPs.

$$\ln K_C = -\frac{\Delta H°}{RT} + \frac{\Delta S°}{R} \tag{5}$$

$$\Delta G° = \Delta H° - T\Delta S° \tag{6}$$

T and R represent the temperature of solution and universal gas constant, respectively.

2.4. Adsorption kinetic parameters

Adsorptions of 10 mL of 35, 65 and 150 mg/L BB dye solutions onto 0.02 g of the prepared NiO NPs were achieved at a rotation speed of 200 rpm, original pH and 303 K for different time intervals. Samples after each time period were filtered. The final dye concentrations in the filtrate were measured by means of UV/Visible spectrometer. Eq. (7) was used for calculating the adsorption quantities for each time t (min).

$$q_t = \frac{(C_i - C_t)V}{m} \tag{7}$$

q_t (mg/g) refers to BB amount removed from its liquid at any time. C_i and C_t (mg/L) represent BB concentrations at primary and any time t, respectively. V and m symbolize the solution volume and mass of NiO NPs, in that order.

These processes were carried out to examine impact of the adsorption agitation time and to evaluate kinetic parameters,

Linear expressions for the first order (Eq. (8)), second order (Eq. (9)) [33] and intra-particle distribution (Eq. (10)) kinetic models have been employed for evaluation of the adsorption capacities and adsorption rate constants.

$$\log(q_e - q_t) = \log q_e - K_1 \frac{t}{2.303} \tag{8}$$

$$\frac{t}{q_t} = \frac{1}{K_2 q_e^2} + \frac{t}{q_e} \tag{9}$$

$$q_t = K_{dif} \sqrt{t} + C \tag{10}$$

Since q_e refers to equilibrium adsorption amount; q_t is the amount of BB eliminated from solution after each time intervals. K_1, K_2 and K_{dif} symbolize the rate constants of first order, second order and intra-particle distribution kinetic models, respectively. C is a kinetic parameter that provides idea about the boundary-layer width [34].

2.5. Impact of pH

BB solutions with constant primary concentration (200 mg/L) and different values of pH (2–12) were prepared by adding 0.5 N NaOH or HCl solutions. A pH meter (model: Ross FE 20, USA) was used for measuring the pH values of these solution. A fixed volume (10 mL) of each solution was combined with 0.02 g of NiO NPs in 25 mL amber bottle. The sealed amber bottles were put in shaker incubator and shaken for 3 d at 30°C and 200 rpm agitation speed. Filtration

using filter papers was performed to separate the solid NiO from the mixtures. The supernatant final concentration and the adsorption amount at equilibrium were estimated as described in the adsorption experiments.

3. Results and discussion

3.1. Adsorbent properties

The XRD pattern of NiO NPs is shown in Fig. 1. The characteristic diffraction peaks corresponded to (111), (200), (220), (311) and (222) indicate the monoclinic structure of NiO nanocrystals [35] which was also found to be highly crystalline planes of NiO NPs. The obtained peaks matched with earlier reports [29,36]. The observed interplanar spacing, d_{hkl}, was compared with the data of JCPDS card number of 78-0429. The results obtained in this study are further supported by XRD results obtained from NiO NPs [24,25].

The size and morphology of the synthesized NiO NPs was studied by TEM; a representative image of NiO nanomaterial is displayed in Fig. 2. The synthesized NiO nanoparticles were mostly spherical in shape and showed a large distribution of sizes, with mean values of 13 ± 2 nm. Similarly, Rabieh et al. [37] highlighted that microwave-assisted synthesis of ZnO NPs was hexagonal with an average size ranging from 15 to 25 nm while Fakhri and Behrouz [21] reported spherical γ-Fe$_2$O$_3$/NiO nanocomposite with size ranging from 55 nm, respectively. Further, Fakhri and Behrouz [21] reported that TEM images of MgO nanoparticles and ZnO–MgO nanocomposites were spheroidal in shape with an average size ranging from 25 to 30 nm. The pH$_{ZPC}$ and the BET surface analyzer values of NiO NPs are listed in Table 2.

3.2. Factors affecting the adsorption

3.2.1. Initial concentration of BB and temperature of solution

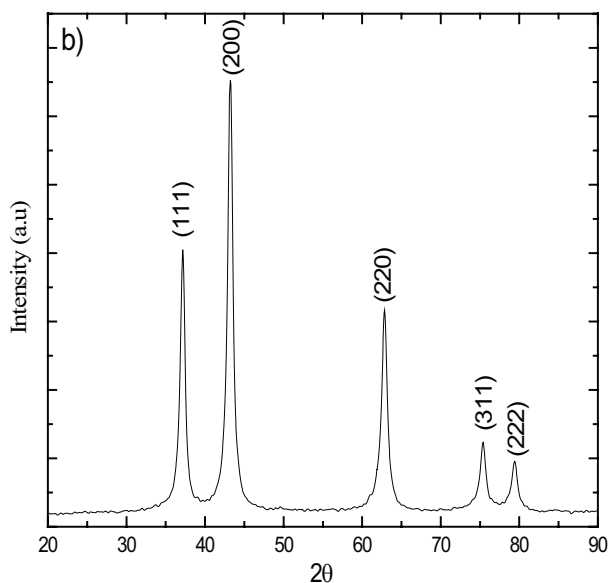Plots of q_e (mg/g) vs. C_i (Fig. 3) represent the impact of primary concentration on the uptake of BB by NiO NPs at three different temperatures (30°C, 45°C and 60°C). Fig. 3 illustrates that adsorption of BB increases with increment in initial concentration of this dye due to the dynamic force that can defeat the mass movement resistances of BB particles at the solid and liquid interface is raised with increasing the primary adsorbate concentration [38,39]. Fig. 3 also demonstrates that the amounts of this dye adsorbed become constant over 300 mg/L at each temperature. This was obtained
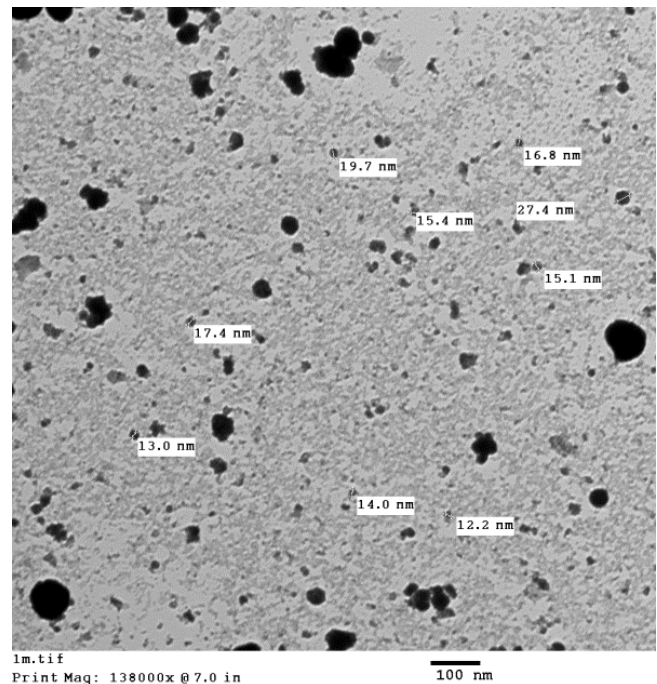
Fig. 2. TEM spectrum of as-prepared NiO NPs.

Table 2
Characteristics of the NiO NPs

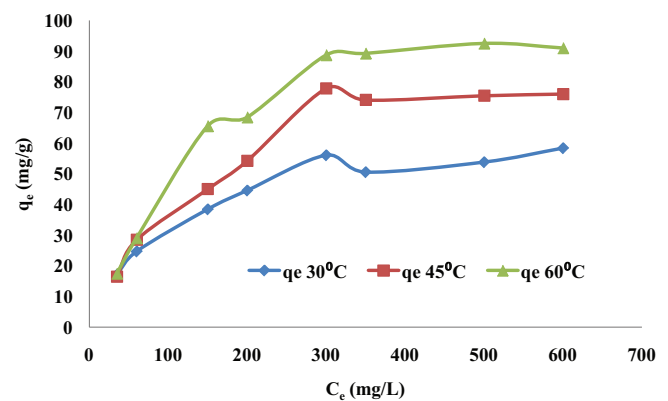| Properties	Valued
Specific surface area (m²/g)	78.3733
Total pore volume (cm³/g)	0.06842
Average pore diameter (Å)	34.920
pH$_{ZPC}$	8.1

Fig. 1. XRD spectrum of as-prepared NiO NPs.

Fig. 3. Effect of initial concentration and temperature on adsorption capacity of BB by NiO NPs.

because there are no vacant active sites on the surface of NiO NPs to adsorb extra of BB molecules when the concentration of this adsorbate is enhanced over 300 mg/L [38,39]. Similar trends were observed for adsorption of acid red 27 dye onto commercial activated carbon granular and coconut husk fibre-based activated carbon [40]. It was reported previously that the amount and percentage of BB removed from aqueous solution by adsorption on activated carbon prepared from *Astragalus bisulcatus tree* were increase by increasing the initial dye concentration [8]. Furthermore, it was observed that adsorption capacity of BB on Sorel's cement NPs increased from 2.84 to 25.14 mg/g when the initial concentration of this dye increased from 2.84 to 25.14 mg/L [23]. Moreover, Fig. 3 shows that the adsorption of BB onto NiO NPs is increased with elevating temperature from 30°C to 60°C. This means that the adsorption of BB onto the surface of NiO NPs is an endothermic process. Increment in the adsorption uptake of BB by raising temperature was resulted from the rising in the mobility of BB molecules [41]. Moreover, sufficient energy is needed for other numbers of BB particle to adsorb onto adsorption active sites [41]. Similar trends were observed for adsorption of this dye on α-chitin NPs [11]. It was also found in the literature that MB adsorption onto commercial activated carbon is an endothermic process in nature [42].

3.2.2. Adsorption agitation time

The relationship between the amounts of BB uptake (q_t mg/g) by NiO NPs at various primary concentrations (35, 65 and 150 mg/L) and agitation time is illustrated in Fig. 4. As shown in Fig. 4, quantity of BB adsorbed onto NiO NPs enhanced with an increase in adsorption contact time and almost be constant after 180 min. The results detected in this research are similar to that obtained for elimination of 4-nitrophenol from aqueous solution by means of its adsorption onto palm oil fuel ash refluxed with amino silane coupling agent [43].

3.2.3. Adsorbate solution pH

Adsorbate ionization degree and adsorbent surface charge are extensively affected by pH of the experimental solution [44]. If pH is higher than the adsorbate pK_a, the adsorbate exists in the ion form [44]. Moreover, in the case of $pH_{ZPC} > pH$ and $pH_{ZPC} < pH$, adsorbent surface will be
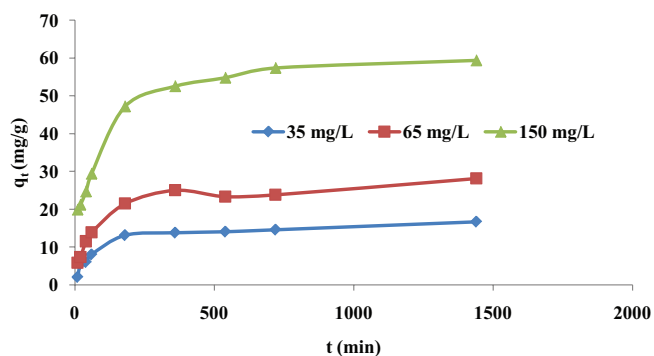
positively and negatively charged, respectively [44]. Fig. 5 represents the plot of BB adsorbed at equilibrium (q_e, mg/g) and solution pH. This figure demonstrates that the adsorption capacity of BB ($pK_a = 3.85$) on NiO ($pH_{ZPC} = 8.1$) is faintly and sharply increased with increasing solution pH in the range of 2–8 and 8–12, respectively. The slight increase in the adsorption of this dye at pH less than 8 was due to the competition adsorption between the positive ions of BB and hydrogen ions. Where increasing the solution pH leads to decreasing the number of hydrogen ions. Therefore, the competition between the ions of BB and hydrogen will be decreased and the adsorption of BB will slightly increase. Whereas, the sharp increment in the adsorption of BB when pH ranged from 8 to 12 was due to increasing the electrostatic attraction forces between BB positive ions and negative charges on the surface of NiO NPs. While, the number of negative surface charges was increased with increasing solution pH, leading to increment in the number of BB ions uptake onto the adsorption active sites. Similar results were noted for adsorption of BB by Sorel's cement NPs [23]. Moreover, the results observed in this research confirm that the maximum amount of BB adsorbed onto NiO NPs can be obtained at increasing pH, which agrees well with those observed for adsorption of MB by Fe_3O_4-graphene@mesoporous SiO_2 nanocomposite and cotton stalk [44,45].

3.3. Isotherm data analysis

Isotherm parameters were analyzed at 30°C, 45°C and 60°C using isotherm models Freundlich and Langmuir. The plots related to Langmuir equation are demonstrated in Fig. 6, whereas Fig. 7 illustrates the plots associated with Freundlich equation. Slopes and intercepts of these plots were used to evaluate isotherm parameters of Langmuir (q_{max}, K_L) and Freundlich (K_F, n). The values of isotherm constants and their equivalent R^2 are listed in Table 3. The R_L values were calculated by Eq. (4) (Table 3).

The isotherms data summarized in this table designate that adsorption of BB by NiO NPs is favourable under the experimental conditions because the values of R_L and $1/n$ are between 0 and 1. The R^2 values of Langmuir isotherm model are superior to that of Freundlich. These results along

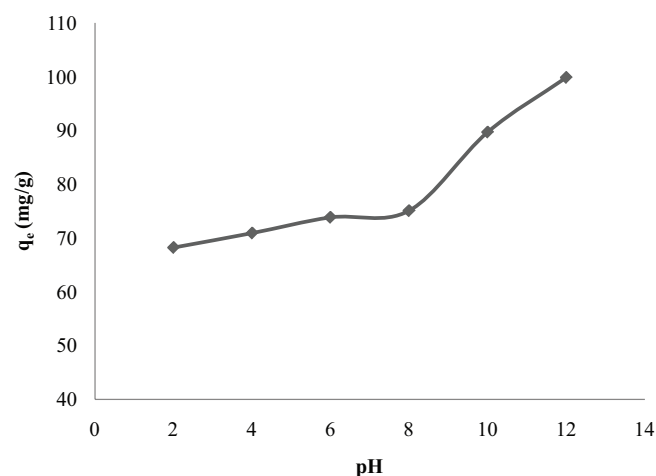Fig. 4. Effect of contact time on the adsorption capacity of BB by NiO NPs.

Fig. 5. Effect of pH on BB adsorption by NiO NPs.

with Figs. 6 and 7 confirm that isotherm model of Langmuir is the best model that can be used to analyze the experimental isotherms data obtained in this study. This clearly indicates that adsorption active sites on the surface of NiO NPs are homogeneous and the adsorption of BB by this adsorbent (NiO NPs) is a monolayer. It was reported in the literatures that adsorption of BB on activated carbon produced from *Astragalus bisulcatus* tree [8] and α-chitin NPs [11] give strong positive indication on the fitness of experimental data of BB adsorption by Langmuir model. It was observed previously that experimental data for adsorption of phenolic compounds such as 4-nitrophenol on commercial and fibre activated carbons give a good fit of the Langmuir isotherm [46].

Moreover, it can be noted from Table 3 that the solution temperature has a positive effect towards q_{max} (mg/g) indicating that BB adsorption by NiO NPs is endothermic in nature. These results agree well with that observed in section 3.2.1. It also can be seen from Table 3 that NiO NPs have higher adsorption capacities towards BB which range from 58.48 to 93.46 mg/g when temperature increased in the range of 30°C–60°C. This confirms that NiO NPs will be a promising material for the treatment of water dyestuff pollution.

3.4. Thermodynamic parameters

Fig. 8 demonstrates the relationship between $\ln K_c$ and $1/T$ (Eq. (5)) for adsorption of BB onto NiO NPs at three different dye concentrations, that is, 200, 300 and 500 mg/L. The slopes and intercepts of these plots have been used for determining the values of $\Delta H°$ and $\Delta S°$, respectively. The values of $\Delta G°$ were calculated from Eq. (6) using $\Delta H°$ and $\Delta S°$ values. The calculated values of $\Delta H°$, $\Delta S°$ and $\Delta G°$ are registered in Table 4. The values of $\Delta H°$ parameter are positive indicating that BB adsorption by NiO NPs is an endothermic process. This agrees well with the results observed in the parts which are associated with the adsorption isotherms and solution temperature impacts. Furthermore, it can be seen from Table 4 that the smallest value of $\Delta H°$ is higher than 20.9 kJ/mol which designates that this dye adsorption onto NiO NPs is chemisorption [47,30].

The positive values of $\Delta S°$ confirm that the randomness in the interface between adsorbent and solution is
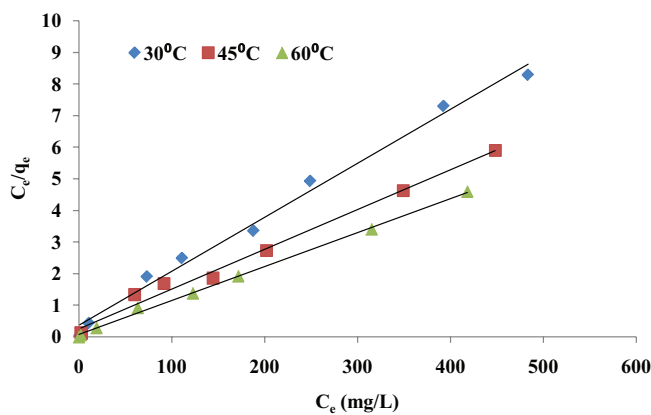
Fig. 6. Langmuir isotherm models for adsorption of BB onto NiO NPs at three different temperatures.
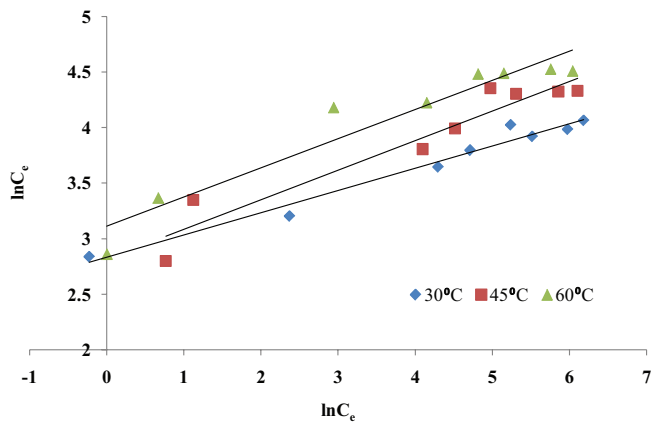
Fig. 7. Freundlich isotherm model for adsorption of BB onto NiO NPs at three different temperatures.
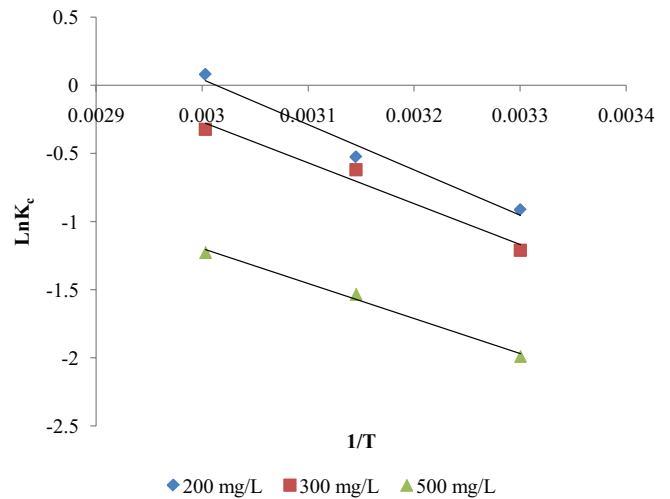
Fig. 8. Plots of $\ln K_c$ vs. $1/T$ for the adsorption of BB onto NiO NPs at three different dye concentrations.

Table 3
Langmuir, Freundlich parameters and separation factors (R_L) for the adsorption of BB dye onto NiO NPs at three different temperatures

Adsorbent	Temperature °C	Langmuir isotherm				Freundlich isotherm			
		q_{max} (mg/g)	K_L (L/mg)	R_L	R^2	K_F (mg/g)(L/mg)$^{1/n}$	$1/n$	n	R^2
NiO NPs	30	58.48	0.046	0.035	0.991	16.99	0.200	5.00	0.971
	45	79.37	0.050	0.032	0.990	18.10	0.251	3.98	0.709
	60	93.46	0.132	0.012	0.998	22.52	0.262	3.81	0.921

Table 4
Thermodynamic parameters for adsorption of BB onto NiO NPs

Adsorbent	Concentration (mg/L)	$\Delta H°$ (kJ/mol)	$\Delta S°$ (kJ/mol K)	$\Delta G°$ (kJ/mol)			
				303 K	318 K	333 K	R^2
NiO NPs	200	27.689	0.082	2.84	1.61	0.383	0.977
	300	24.921	0.073	2.80	1.701	0.61	0.973
	500	21.381	0.054	5.02	4.21	3.40	0.993

decreased through adsorption procedure. According to $\Delta G°$ positive values, BB adsorption by NiO NPs is a non-spontaneous process. Furthermore, it can be observed from Table 4 that $\Delta G°$ values decreased with raising temperature. This proposes that the main approving factor for effective adsorption performance is a higher temperature in this case. Sohni et al. [9] reported that adsorption of BB on magnetic chitosan–graphene oxide composites is an endothermic process.

3.5. Kinetic data analysis

The linearized-integral forms of first order (Eq. (8)), second order (Eq. (9)) and intra-particle diffusion kinetic models (Eq. (10)) have been employed to investigate the kinetic data for adsorption of BB onto NiO NPs. Figs. 9–11 represent the plots of $\log(q_e - q_t)$ vs. t, t/q_t vs. t and q_t vs. $t^{1/2}$, respectively. Slopes and intercepts of these plots were used for determining the kinetic parameters of each model. The experimental q_{max} values along with values of kinetic parameters for the first and second order kinetic models are summarized in Table 5. The calculated R^2 values associated with first and second order kinetic models are also registered in Table 5. It can be observed from Table 5 that correlation coefficients (R^2) values in case of the second order are higher than that of first order. Moreover, the calculated values of q_e using second order kinetic model agree well with the experimental data of q_e. This indicates that the experimental data observed in this study are described well by second order kinetic model. These results confirm that adsorption of BB by NiO NPs is chemisorption as suggested previously in the thermodynamic studies [48].

The kinetic parameters (K_{dif} and C) of intra-particle kinetic model were also computed and registered along with regression coefficient values (R^2) in Table 6. Values of R^2 for most of the plots are smaller than 0.9 and the C values are higher than 0. Furthermore, it can be observed from Fig. 11 that the plots were not linear over the full time range and separated into two linear regions. This designates that the adsorption of BB on NiO NPs has been performed by multiple steps. Additionally, the lines do not pass through the origin, which proposes that intra-particle diffusion is not the rate controlling step. Similar results have been reported by Lafi and Hafiane [49].

3.6. Comparison of performance of NiO NPs with reported adsorbents

The maximum adsorption capacities of NiO NPs along with that of the other adsorbent have been used in the literatures for removal of BB from aqueous media were
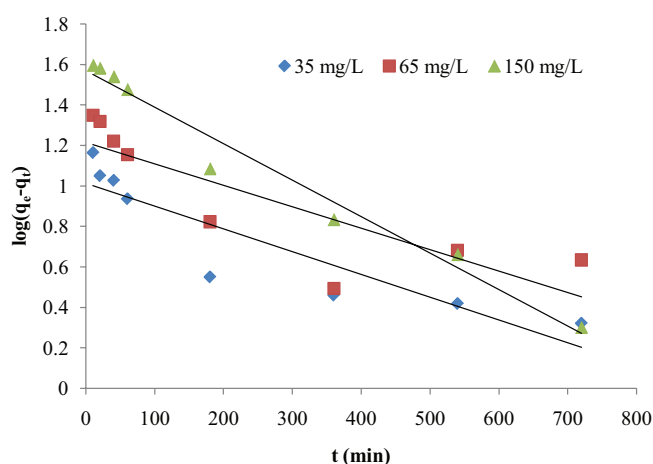

Fig. 9. Pseudo-first-order kinetic model for adsorption of BB onto NiO NPs.
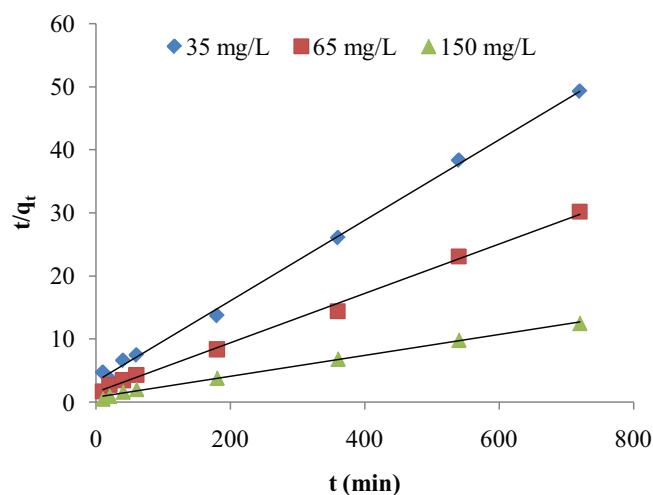

Fig. 10. Pseudo-second-order kinetic model for adsorption of BB onto NiO NPs.

summarized in Table 7 to demonstrate the importance of NiO NPs used in this work comparing with others. This table shows that NiO NPs have adsorption performance higher than that of other which indicates that this adsorbent NPs will meet a significant interest in the case of water purification activities.

4. Conclusion

This study focused the adsorption of BB on NiO NPs at three different temperatures. First, NiO NPs were prepared

Table 5
Pseudo-first and pseudo-second order parameters and experimental q_e values for the adsorption of BB by NiO NPs at different initial concentrations and 30°C ± 1°C

Adsorbent	C_0 (mg/L)	$q_{e,\exp}$ (mg/g)	Pseudo-first order kinetic model			Pseudo-second order kinetic model			
			$q_{e,\text{cal}}$ (mg/g)	K_1 (h^{-1})	R^2	$q_{e,\text{cal}}$ (mg/g)	K_2 (g/mg min)	R^2	Rate
NiO NPs	35	16.713	10.31	0.003	0.826	15.65	0.0012	0.998	0.019
	65	28.183	16.41	0.003	0.715	28.49	0.0005	0.993	0.014
	150	59.409	37.06	0.004	0.974	60.24	0.0003	0.997	0.018

Table 6
Parameter values of intra-particle diffusion model for the adsorption of BB by NiO NPs at different initial concentrations and 30°C ± 1°C

Adsorbent	C_0 (mg/L)	$q_{e,\exp}$ (mg/g)	Intra-particle diffusion kinetic model		
			K_{dif} (mg/h$^{1/2}$ g)	C	R^2
NiO NPs	35	16.713	0.492	3.281	0.849
	65	28.183	0.792	6.262	0.843
	150	59.409	1.718	16.068	0.934
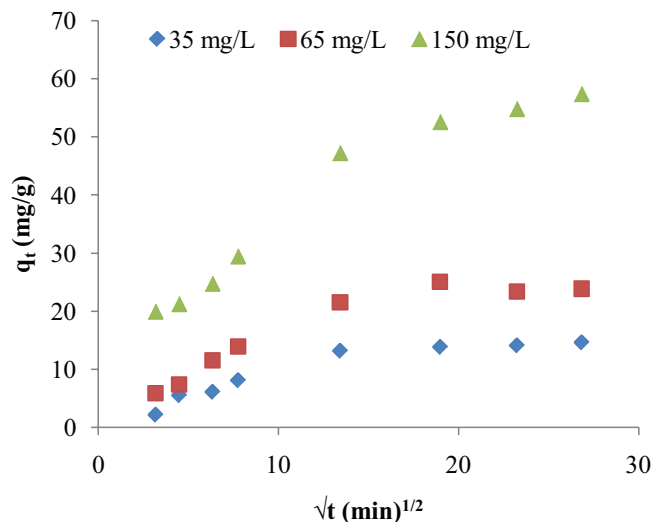
Fig. 11. Intra-particle diffusion model for adsorption of BB onto NiO NPs.

Table 7
Comparison of adsorption capacity of NiO NPs used as adsorbent in this study with other adsorbents towards BB

Adsorbent	$q_{\max}$ (mg/g)		Sources
α-Chitin	22.72		[11]
Sorel's cement NPs	16.39		[23]
Activated carbon	1.89		[50]
Activated carbon	51.21	0.5 g of AC	[8]
	43.89	1.0 g of AC	
	28.54	1.5 g of AC	
	23.45	2.0 g of AC	
Alumina	6.36	25°C	[22]
	5.70	30°C	
	5.64	35°C	
	4.56	40°C	
	2.92	45°C	
Magnetic chitosan–graphene oxide composite	28		[9]
Polymeric gels	2.99		[12]
Hybrid gel	26.40	25°C	[13]
	26.00	50°C	
	27.50	75°C	
Fe_2O_3–ZnO–$ZnFe_2O_4$/carbon nanocomposite	90.91		[16]
NiO NPs	58.48	30°C	Present research
	79.37	45°C	
	93.46	60°C	

and identified by means of BET analysis, TEM and XRD. Initial dye concentration, agitation time, solution temperature and pH have significant effect on the adsorption performance. The adsorption optimal conditions are the temperature of 60°C, pH of 12 and 300 mg/L of adsorbate initial concentration. The results confirm the significant ability of NiO NPs to uptake the tested dye from synthesized wastewater. The Langmuir isotherm model is strongly able to fit and describe experimental data with adsorption capacities of 58.48, 79.37 and 93.46 mg/g at 30°C, 45°C and 60°C, respectively. Adsorption rate was quite fast and the experimental data are described well by a second order kinetic model. Intra-particle diffusion mechanism was complicated in case of BB adsorption by NiO NPs at each concentration. Thermodynamic parameters such as $\Delta H°$, $\Delta S°$ and $\Delta G°$ indicate that BB adsorption using this adsorbent is an endothermic process.

References

[1] L. Yu-Juan, Z. Xi-Hai, Removal of organic-dye (bromophenol blue) by solvent solution, Chem. J. Chin. Univ., 21 (2000) 76–76.

[2] Y. Lu, Y. Wang, X. Zhu, The removal of bromophenol blue from water by solvent solution, Sep. Sci. Technol., 36 (2001) 3763–3776.

[3] R. Azmat, Z. Khalid, M. Haroon, K.B. Mehar, Spectral analysis of catalytic oxidation and degradation of bromophenol blue at low pH with potassium dichromate, Adv. Nat. Sci., 6 (2013) 38–43.

[4] J. Yang, S. Cui, J.Q. Qiao, H.Z. Lian, The photocatalytic dehalogenation of chlorophenols and bromophenols by cobalt doped nano TiO_2, J. Mol. Catal. A Chem., 395 (2014) 42–51.

[5] Y. Absalan, I. Bratchikova, O.V. Kovalchukova, Accurate investigation to determine the best conditions for using $NiTiO_3$ for bromophenol blue degradation in the environment under UV-Vis light based on concentration reduction and to compare it with TiO_2, Environ. Nanotechnol. Monit. Manage., 8 (2017) 244–253.

[6] A. Nezamzadeh-Ejhieh, H. Zabihi-Mobarakeh, Heterogeneous photodecolorization of mixture of methylene blue and bromophenol blue using CuO-nano-clinoptilolite, J. Ind. Eng. Chem., 20 (2014) 1421–1431.

[7] N.K. Temel, R. Gürkan, F. Ayan, Photocatalytic TiO_2-catalyzed degradation of bromophenol blue-mediated Mo(VI)-peroxo complexes in the presence of SDS, Desal. Wat. Treat., 57 (2016) 21083–21090.

[8] M. Ghaedi, A.M. Ghaedi, E. Negintaji, A. Ansari, A. Vafaei, M. Rajabi, Random forest model for removal of bromophenol blue using activated carbon obtained from *Astragalus bisulcatus* tree, J. Ind. Eng. Chem., 20 (2014) 1793–1803.

[9] S. Sohni, K. Gul, F. Ahmad, I. Ahmad, A. Khan, N. Khan, S.B. Khan, Highly efficient removal of acid red-17 and bromophenol blue dyes from industrial wastewater using graphene oxide functionalized magnetic chitosan composite, Polym. Compos. (2017). doi: 10.1002/pc.24349.

[10] L. Ai, L. Li, Efficient removal of organic dyes from aqueous solution with ecofriendly biomass-derived carbon@ montmorillonite nanocomposites by one-step hydrothermal process, Chem. Eng. J., 223 (2013) 688–695.

[11] S. Dhananasekaran, R. Palanivel, S. Pappu, Adsorption of methylene blue, bromophenol blue, and coomassie brilliant blue by α-chitin nanoparticles, J. Adv. Res., 7 (2016) 113–124.

[12] M.A. Malana, S. Ijaz, M.N. Ashiq, Removal of various dyes from aqueous media onto polymeric gels by adsorption process: their kinetics and thermodynamics, Desalination, 263 (2010) 249–257.

[13] L. You, Z. Wu, T. Kim, K. Lee, Kinetics and thermodynamics of bromophenol blue adsorption by a mesoporous hybrid gel derived from tetraethoxysilane and bis (trimethoxysilyl) hexane, J. Colloid Interface Sci., 300 (2006) 526–535.

[14] J. Liu, S. Yao, L. Wang, W. Zhu, J. Xu, H. Song, Adsorption of bromophenol blue from aqueous samples by novel supported ionic liquids, J. Chem. Technol. Biotechnol., 89 (2014) 230–238.

[15] H. Mazaheri, M. Ghaedi, A. Asfaram, S. Hajati, Performance of CuS nanoparticle loaded on activated carbon in the adsorption of methylene blue and bromophenol blue dyes in binary aqueous solutions: using ultrasound power and optimization by central composite design, J. Mol. Liq., 219 (2016) 667–676.

[16] A. Mohammadzadeh, M. Ramezani, A.M. Ghaedi, Synthesis and characterization of Fe_2O_3-ZnO-$ZnFe_2O_4$/carbon nanocomposite and its application to removal of bromophenol blue dye using ultrasonic assisted method: optimization by response surface methodology and genetic algorithm, J. Taiwan Inst. Chem. Eng., 59 (2016) 275–284.

[17] A.A. El-Zahhar, N.S. Awwad, E.E. El-Katori, Removal of bromophenol blue dye from industrial waste water by synthesizing polymer-clay composite, J. Mol. Liq., 199 (2014) 454–461.

[18] A. Fakhri, Investigation of mercury (II) adsorption from aqueous solution onto copper oxide nanoparticles: optimization using response surface methodology, Process Saf. Environ. Prot., 93 (2015) 1–8.

[19] A. Fakhri, Assessment of Ethidium bromide and Ethidium monoazide bromide removal from aqueous matrices by adsorption on cupric oxide nanoparticles, Ecotoxicol. Environ. Saf., 104 (2014) 386–392.

[20] A. Fakhri, Application of response surface methodology to optimize the process variables for fluoride ion removal using maghemite nanoparticles, J. Saudi Chem. Soc., 18 (2014) 340–347.

[21] A. Fakhri, S. Behrouz, Comparison studies of adsorption properties of MgO nanoparticles and ZnO–MgO nanocomposites for linezolid antibiotic removal from aqueous solution using response surface methodology, Process Saf. Environ. Prot., 94 (2015) 37–43.

[22] M.J. Iqbal, M.N. Ashiq, Thermodynamics and kinetics of adsorption of dyes from aqueous media onto alumina, J. Chem. Soc. Pak., 12 (2010) 419–428.

[23] S.M.A. El-Gamal, M.S. Amin, M.A. Ahmed, Removal of methyl orange and bromophenol blue dyes from aqueous solution using Sorel's cement nanoparticles, J. Environ. Chem. Eng., 3 (2015) 1702–1712.

[24] H. Hu, G. Chen, C. Deng, Y. Qian, M. Wang, Q. Zheng, Green microwave-assisted synthesis of hierarchical NiO architectures displaying a fast and high adsorption behavior for Congo red, Mater. Lett., 170 (2016) 139–141.

[25] Y. Zheng, B. Zhu, H. Chen, W. You, C. Jiang, J. Yu, Hierarchical flower-like nickel (II) oxide microspheres with high adsorption capacity of Congo red in water, J. Colloid Interface Sci., 504 (2017) 688–696.

[26] C. Lei, X. Zhu, B. Zhu, J. Yu, W. Ho, Hierarchical NiO–SiO_2 composite hollow microspheres with enhanced adsorption affinity towards Congo red in water, J. Colloid Interface Sci., 466 (2016) 238–246.

[27] Y.B. Shao, J.H. Huang, Synthesis and adsorption study of nanobelts for removal of anionic dyes, Desal. Wat. Treat., 65 (2017) 327–336.

[28] M.H. Mahmoud, A.M. Elshahawy, S.A. Makhlouf, H.H. Hamdeh, Mossbauer and magnetization studies of nickel ferrite nanoparticles synthesized by the microwave combustion method, J. Magn. Magn. Mater., 343 (2013) 21–26.

[29] R.W. Cairns, E. Ott, X-Ray Studies of the system nickel-oxygen-water. I. Nickelous oxide and hydroxide, J. Am. Chem. Soc., 55 (1933) 527–533.

[30] S.K. Theydan, M.J. Ahmed, Adsorption of methylene blue onto biomass-based activated carbon by $FeCl_3$ activation: equilibrium, kinetics, and thermodynamic studies, J. Anal. Appl. Pyrol., 97 (2012) 116–122.

[31] G. Atun, G. Hisarli, W.S. Sheldrick, M. Muhlerler, Adsorptive removal of methylene blue from colored effluents on fuller's earth, J. Colloid Interface Sci., 261 (2003) 32–39.

[32] T.W. Weber, P. Chakkravorti, Pore and solid diffusion models for fixed-bed adsorbers, AIChE J., 20 (1974) 220–228.

[33] Y.S. Ho, Review of second-order models for adsorption systems, J. Hazard. Mater., 136 (2006) 681–689.

[34] F. Ahmad, W.M.A.W. Daud, M.A. Ahmad, R. Radzi, Using cocoa (*Theobroma cacao*) shell-based activated carbon to remove 4-nitrophenol from aqueous solution: kinetics and equilibrium studies, Chem. Eng. J., 178 (2011) 461–467.

[35] W.T. Yao, S.H. Yu, Y. Zhou, Formation of uniform CuO nanorods by spontaneous aggregation: selective synthesis of CuO, Cu_2O, and Cu nanoparticles by a solid-liquid phase arc discharge process, J. Phys. Chem. B, 109 (2005) 14011–14016.

[36] L.G. Teoh, K.D. Li, Synthesis and characterization of NiO nanoparticles by sol–gel method, Mater. Trans., 53 (2012) 2135–2140.

[37] S. Rabieh, M.N. Bagheri, M. Heydari, E. Badiei, Microwave assisted synthesis of ZnO nanoparticles in ionic liquid [Bmim] cl and their photocatalytic investigation, Mater. Sci. Semicond. Process., 26 (2014) 244–250.

[38] Q. Baocheng, Z. Jiti, X. Xuemin, Z. Chunli, Z. Hongxia, Z. Xiaobai, Adsorption behavior of Azo Dye C. I. Acid Red 14 in aqueous solution on surface soils, J. Environ. Sci., 20 (2008) 704–709.

[39] V.K. Gupta, B. Guptaa, A. Rastogi, S. Agarwal, A. Nayak, A comparative investigation on adsorption performances of

mesoporous activated carbon prepared from waste rubber tire and activated carbon for a hazardous azo dye-Acid Blue 113, J. Hazard. Mater., 186 (2011) 891–901.

[40] H.A. AL-Aoh, M.J. Maah, R. Yahya, M.R. Bin Abas, A comparative investigation on adsorption performances of activated carbon prepared from coconut husk fiber and commercial activated carbon for acid red 27 dye, Asian J. Chem., 25 (2013) 9582–9590.

[41] B.H. Hameed, A.A. Ahmad, Batch adsorption of methylene blue from aqueous solution by garlic peel, an agricultural waste biomass, J. Hazard. Mater., 164 (2009) 870–875.

[42] H.A. AL-Aoh, R. Yahya, M.J. Maah, M.R. Bin Abas, Adsorption of methylene blue on activated carbon fiber prepared from coconut husk: isotherm, kinetics and thermodynamics studies, Desal. Wat. Treat., 52 (2014) 6720–6732.

[43] H.A. AL-Aoh, M.J. Maah, A.A. Ahmad, M.R. Bin Abas, Adsorption of 4-nitrophenol on palm oil fuel ash activated by amino silane coupling agent, Desal. Wat. Treat., 40 (2012) 159–167.

[44] X.L. Wu, Y. Shi, S. Zhong, H. Lin, J.R. Chen, Facile synthesis of Fe_3O_4-graphene@mesoporous SiO_2 nanocomposites for efficient removal of Methylene Blue, Appl. Surf. Sci., 378 (2016) 80–86.

[45] H. Deng, J. Lu, G. Li, G. Zhang, X. Wang, Adsorption of methylene blue on adsorbent materials produced from cotton stalk, Chem. Eng. J., 172 (2011) 326–334.

[46] H.A. AL-Aoh, M.J. Maah, R. Yahya, M.R. Bin Abas, Isotherms, kinetics and thermodynamics of 4-nitrophenol adsorption on fiber-based activated carbon from coconut husks prepared under optimized conditions, Asian J. Chem., 25 (2013) 9573–9581.

[47] A. Kurniawan, S. Ismadji, Potential utilization of *Jatropha curcas* L. press-cake residue as new precursor for activated carbon preparation: application in methylene blue removal from aqueous solution, J. Taiwan Inst. Chem. Eng., 42 (2011) 826–836.

[48] S.F. Soares, T.R. Simões, T. Trindade, A.L. Daniel-da-Silva, Highly efficient removal of dye from water using magnetic carrageenan/silica hybrid nano-adsorbents, Water Air Soil Pollut., 228 (2017) 87.

[49] R. Lafi, A. Hafiane, Removal of methyl orange (MO) from aqueous solution using cationic surfactants modified coffee waste (MCWs), J. Taiwan Inst. Chem. Eng., 58 (2016) 424–433.

[50] A.O. Dada, A.A. Inyinbor, A.P. Oluyori, Comparative adsorption of dyes onto activated carbon prepared from maize stems and sugar cane stems, IOSR J. Appl. Chem., 2 (2012) 38–43.